

Article

Numerical Investigation on Temporal Evolution Behavior for Triad Resonant Interaction Induced by Steady Free-Surface Flow over Rippled Bottoms

Jun Fan ^{1,2} , Aifeng Tao ^{1,2,*}, Jinhai Zheng ^{1,2} and Ji Peng ³

¹ Key Laboratory of Ministry of Education for Coastal Disaster and Protection, Hohai University, Nanjing 210024, China

² College of Harbour, Coastal and Offshore Engineering, Hohai University, Nanjing 210024, China

³ China Renewable Energy Engineering Institute, Beijing 100120, China

* Correspondence: aftao@hhu.edu.cn; Tel.: +86-152-9554-0618

Abstract: Investigating the wave hydrodynamics of free-surface flow over rippled bottoms is a continuing concern due to the existence of submarine multiple sandbars and ambient flow in coastal and estuarial areas. More attention to free-surface wave stimulation has been received from the perspective of resonant wave-wave interaction, which is an intensive way for wave energy transfer and a potential way for wave component generation. However, the basic behavior of the triad resonant interaction of this problem is still limited and unclear. In this study, the triad resonant interaction induced by steady free-surface flow over rippled bottoms is numerically investigated by means of the High-Order Spectral (HOS) method. By considering the interactions among free-surface waves, ambient current, and rippled bottoms, the numerical model is applied for this situation based on Zakharov equation with ambient flow term. The temporal evolution of the triad resonant wave amplitude has been numerically investigated and compared well with multiple-scale expansion perturbation theory. Specifically, the temporal evolution behaviors of all six triad resonant wave components are confirmed by both numerical simulation and nonlinear perturbation analysis.

Keywords: triad resonant interaction; numerical simulation; high-order spectral method (HOS); free-surface flow; temporal instability



Citation: Fan, J.; Tao, A.; Zheng, J.; Peng, J. Numerical Investigation on Temporal Evolution Behavior for Triad Resonant Interaction Induced by Steady Free-Surface Flow over Rippled Bottoms. *J. Mar. Sci. Eng.* **2022**, *10*, 1372. <https://doi.org/10.3390/jmse10101372>

Academic Editor: Luca Cavallaro

Received: 15 August 2022

Accepted: 22 September 2022

Published: 26 September 2022

Publisher's Note: MDPI stays neutral with regard to jurisdictional claims in published maps and institutional affiliations.



Copyright: © 2022 by the authors. Licensee MDPI, Basel, Switzerland. This article is an open access article distributed under the terms and conditions of the Creative Commons Attribution (CC BY) license (<https://creativecommons.org/licenses/by/4.0/>).

1. Introduction

The open channel flow over rippled bottoms has drawn increasing attention to wave hydrodynamics recently [1–3] because the possible unstable resonant modes might be triggered in some circumstances of ambient flow and bottom ripples. It will be applied in the research of the estuarial wave field due to the existence of continuous submarine sandbars and ambient tidal/runoff currents.

Firstly, the related studies of the resonant interaction with the existence of ambient flow and rippled bottoms originated from the early study of stationary waves for free-surface flow over rippled bottoms [4–7]. This steady-state free-surface wavy profile becomes an important part of introducing the following resonant-related work because the stationary waves are the medium for achieving the resonant interaction and energy transition from ambient flow (with rippled bottoms) to free-surface propagating (resonance-related) wave components.

Then, the theory of resonant wave-wave interaction [8–10] was introduced to the problem of steady free-surface flow over rippled bottoms. The leading-order (triad interaction at second order) resonance became a critical issue to discuss the potential unstable resonant wave modes. If the leading-order resonance with unstable resonant modes is triggered, the wave energy transfer induced by resonance will be very intensive and the free surface wave field could be strongly affected in estuarial areas with the existence of continuous

submarine sandbars and ambient currents. It was first proposed from the perspective of instability of stationary waves for steady free-surface flow over rippled bottoms [11]. By linear instability analysis, it reveals that the stationary waves are unstable for any bottom wavenumber if the Froude number $F \geq 1$, and for bottom wavenumber $k_b > k_{bc}$ (k_{bc} as the critical value) if $F < 1$.

Further, McHugh [12] investigated the stability of stationary waves for steady free-surface flow along the channel with rippled sidewalls. During the analysis of the condition for unstable wave modes, the classification of this specific triad resonance was given.

Specifically, for the triad resonance involving free-surface waves, ambient current, and rippled bottoms, there are totally six triad resonant combinations that correspond to two free-surface resonant wave components (from four wavenumber solutions in currents [13]) and one bottom profile steady wave component.

In detail, for the triad resonance induced by free-surface uniform flow (U) over rippled bottoms, two free-surface propagating wave components and one bottom wave component (fixed bottom) are involved. These two free-surface resonant wave components have different wavenumbers (k_m and k_n) and the same frequency ($\omega_m = \omega_n = \omega$) in general. The bottom resonant wave component is steady with zero frequency and wavenumber k_b for the bottom profile. Under the assumption of $\omega > 0$ and $k_b > 0$ without loss of generality, the triad resonant conditions will be satisfied as below.

$$k_m - k_n = \pm k_b \text{ and } \omega_m - \omega_n = 0 \tag{1}$$

The wavenumbers (k_m and k_n) and frequency ($\omega_m = \omega_n = \omega$) of the free-surface resonant wave components satisfy the dispersion relation with the uniform ambient current.

$$(\omega - kU)^2 = gk \tanh kh \tag{2}$$

in which $k = k_m$ or k_n . From this dispersion relation with the given free-surface wave frequency, there are four wavenumber solutions in total [13] ($k_1 \sim k_4$) obtained at most (as referred to in [2] Figure 2). Then, the subscripts become $m, n = 1, 2, 3, 4$ and $m \neq n$.

The wavenumber solutions of k_3 and k_4 always exist with positive values ($0 < k_3 < k_4$), which means that the phases of k_3 and k_4 wave components are traveling along with the flow. However, the wavenumber solutions of k_1 and k_2 are negative ($k_2 \leq k_1 < 0$) but do not always exist (only exist if the flow velocity is less than the critical value), which means that the phases of k_1 and k_2 wave components are traveling against the flow. For the wave energy propagation, the wave energy of k_2, k_3 , and k_4 propagates downstream, whereas the wave energy of k_1 propagates upstream.

If all four resonant wavenumber solutions exist with a given wave frequency ω and flow velocity U , there will be six triad resonant combinations in total: Triad resonant combinations (1): $k_3 - k_1 = k_b$; (2): $k_3 - k_2 = k_b$; (3): $k_4 - k_3 = k_b$; (4): $k_4 - k_2 = k_b$; (5): $k_4 - k_1 = k_b$; (6): $k_1 - k_2 = k_b$.

On the basis of above, the temporal instability scenario for stationary waves discussed by Yih [11] only belongs to one specific triad resonant combination (3) containing two downstream-propagating resonant wave components (k_3 and k_4).

Moreover, the effects on the instability condition of surface tension were considered [14]. It concludes that for zero surface tension, the waves from three triad resonant combinations (expressed as p waves, which correspond to triad combinations No. 1–3) are always unstable. Later, the phenomenon of upstream-propagating waves for flow over rippled bottoms was observed by flume experiments [15,16]. The generation mechanisms are analyzed by multiple-scale expansion perturbation from the perspective of triad resonance and validated by experiments [2]. However, it is still of limited understanding for the temporal evolution behavior of triad resonant interactions for free-surface flow over rippled bottoms.

In this study, we focus on six triad resonant combinations induced by free-surface steady and uniform flow over rippled bottoms. The High-Order Spectral (HOS) method numerical model is established to investigate the temporal evolution characteristics of

triad resonant free-surface wave components for flow over rippled bottoms. The specific objective of this study was to identify the temporal evolution behavior of all six triad resonant combinations and provide clear conclusions, which are cross-validated by numerical simulation results.

The remainder of this paper is organized as follows. The mathematical formulation of the High-Order Spectral (HOS) method for wave-current-bottom interactions is summarized in Section 2. The results of the HOS numerical simulation for temporal evolution, as well as the comparison with perturbation theory for exact triad resonance, are presented in Section 3. Finally, Section 4 contains the discussions and conclusions. Furthermore, the necessary information from the previous studies on instability analyses and multiple-scale expansion perturbation solutions are reviewed in the appendixes.

2. High-Order Spectral Method (HOS) Method for Free-Surface Flow over Rippled Bottoms

The High-Order Spectral (HOS) method is applied to calculate the spatial distribution and temporal evolution of resonant waves' amplitudes in this study. This numerical study is initialized for cross-validation between numerical and theoretical solutions of resonant interaction among free-surface waves, rippled bottoms, and ambient (steady and uniform) flow.

The HOS numerical model is based on the ideas of the Zakharov equation [17] and mode-coupling [18]. It was firstly developed for nonlinear wave-wave interaction [19,20], then, it was extended to wave-body interaction [21], wave-bottom interaction [22–24], and many other scenarios [25–27]. This numerical model could solve the nonlinear initial boundary value problem up to any order. Its computational efforts will be kept near linear dependence based on orthogonal spectral expansions for the free-surface and bottom functions as well as fast Fourier transform techniques. The solutions calculated have exponential convergence with an increasing number of free-surface and bottom modes. The HOS model applied to calculate the resonant interaction for free surface waves in the presence of ambient steady uniform flow and rippled bottoms in this study are adapted based on the program developed for investigation of the Bragg resonance (wave-bottom resonant interaction without ambient current [22,23]).

For the mathematical formulation and algorithm of HOS with the existence of ambient flow, in the presence of ambient steady and uniform flow of velocity, the nonlinear free-surface boundary conditions in the Zakharov form [17] are,

$$\eta_t + \eta_x U + \eta_x \Phi_x^S - (1 + \eta_x \eta_x) \Phi_z(x, \eta, t) = 0 \tag{3}$$

$$\Phi_t^S + \frac{1}{2} U^2 + \frac{1}{2} \Phi_x^S \Phi_x^S + \eta - \frac{1}{2} (1 + \eta_x \eta_x) \Phi_z^2(x, \eta, t) = 0 \tag{4}$$

in which the terms $\eta_x U$ and $\frac{1}{2} U^2$ indicate the effect of steady and uniform ambient flow. The function Φ^S is the surface potential defined as below.

$$\Phi^S(x, t) = \Phi(x, \eta(x, t), t) \tag{5}$$

Therefore, Equations (3) and (4) are evolution equations that could be integrated by giving the initial value of surface elevation $\eta(x, 0)$ and free surface potential $\Phi^S(x, \eta(x, 0), 0)$. The surface vertical velocity $\Phi_z(x, \eta(x, t), t)$ could be solved by the boundary conditions.

The bottom boundary condition of the rippled patch at $z = -h + \zeta(x)$ is as below,

$$\Phi_z = \zeta_x (U + \Phi_x) \tag{6}$$

For solving the boundary value problem, the regular perturbation expansion is applied to the velocity potential $\Phi(x, z, t)$. In this paper, if the steepness of free surface elevation

and bottom undulation is assumed to be the identical small value of ϵ , then the velocity potential is expanded as below,

$$\Phi(x, z, t) = \sum_{m=1}^M \Phi^{(m)}(x, z, t) \tag{7}$$

in which $\Phi^{(m)}$ is the velocity potential of each order up to arbitrary order M with $\Phi^{(m)} = O(\epsilon^m)$.

To get the relation of velocity potential $\Phi(x, z, t)$ by each order, the Taylor expansion is applied to the mean free surface $z = 0$ and mean bottom $z = -h$, respectively.

At mean free surface $z = 0$, the expressions of velocity potential by successive orders are obtained as Dirichlet boundary conditions.

$$\Phi^{(1)}(x, 0, t) = \Phi^S \tag{8}$$

$$\Phi^{(m)}(x, 0, t) = - \sum_{\ell=1}^{m-1} \frac{\eta^\ell}{\ell!} \frac{\partial^\ell}{\partial z^\ell} \Phi^{(m-\ell)}(x, 0, t) \quad m = 2, 3, \dots, M \tag{9}$$

At the mean rippled bottom $z = -h$, the expressions of velocity potential by successive orders are obtained as Neumann boundary conditions.

$$\Phi_z^{(1)}(x, -h, t) = U\zeta_x \tag{10}$$

$$\Phi_z^{(m)}(x, -h, t) = \sum_{\ell=1}^{m-1} \frac{\partial}{\partial x} \left[\frac{\zeta^\ell}{\ell!} \frac{\partial^{\ell-1}}{\partial z^{\ell-1}} \Phi_x^{(m-\ell)}(x, -h, t) \right] \quad m = 2, 3, \dots, M \tag{11}$$

Based on the periodic condition of horizontal coordinate x and the Laplace governing equation in the computation domain $-h < z < 0$, the perturbation potential function $\Phi^{(m)}(x, z, t)$ at each order could be decomposed into two kinds of terms which satisfy only the free-surface or bottom boundary condition separately based on the linear superposition of the Laplace operator.

Therefore, we decompose each order's velocity potential $\Phi^{(m)} = \alpha^{(m)} + \beta^{(m)}$. $\alpha^{(m)}$ and $\beta^{(m)}$ satisfy the homogeneous bottom boundary condition (zero Neumann condition) and homogeneous free-surface boundary condition (zero Dirichlet condition), respectively. Then, the decomposed velocity potentials $\alpha^{(m)}$ and $\beta^{(m)}$ are expanded by the eigenfunction of the Fourier series.

$$\alpha^{(m)}(x, z, t) = \sum_{n=0}^{\infty} \alpha_n^{(m)}(t) \frac{\cosh[|\mathbf{k}_n|(z+h)]}{\cosh(|\mathbf{k}_n|h)} e^{i\mathbf{k}_n x} + c.c. \tag{12}$$

$$\beta^{(m)}(x, z, t) = \beta_0^{(m)}(t)z + \sum_{n=1}^{\infty} \beta_n^{(m)}(t) \frac{\sinh[|\mathbf{k}_n|(z+h)]}{|\mathbf{k}_n|\cosh(|\mathbf{k}_n|h)} e^{i\mathbf{k}_n x} + c.c. \tag{13}$$

in which $\alpha^{(m)}$ and $\beta^{(m)}$ are the modal amplitudes which are solved with corresponding boundary conditions.

Thus, the vertical velocity term $\Phi_z(x, \eta, t)$ on the free surface could be obtained from

$$\Phi_z(x, \eta, t) = \sum_{m=1}^M \sum_{\ell=0}^{M-m} \frac{\eta^\ell}{\ell!} \frac{\partial^{\ell+1}}{\partial z^{\ell+1}} \Phi^{(m)}(x, 0, t) \tag{14}$$

Therefore, the vertical velocity term $\Phi_z(x, \eta, t)$ will be solved iteratively during the numerical solving process to obtain the updated value of $\Phi^S(x, t)$ and $\eta(x, t)$ in HOS.

At the initialization of the simulation process, all parameters are dimensionless along with the number of total spatial points N and nonlinear order M . Then, based on the initial free surface elevation function $\eta_0(x)$ and surface potential $\Phi_0^S(x)$, which are already given as the initial condition, the values of modal amplitudes $\alpha_n^{(m)}(t)$ and $\beta_n^{(m)}(t)$ will

be obtained by solving both Dirichlet and Neumann boundary value problems with the pseudo-spectral method.

During the iteration process, the modal amplitudes $\alpha_n^{(m)}(t)$, $\beta_n^{(m)}(t)$ and free surface elevation $\eta(x)$ are substituted into the expression $\Phi_z(x, \eta, t)$ to obtain the vertical velocity on the free surface. Then, the value of $\Phi_z(x, \eta, t)$ is substituted into the evolution equation to obtain the time derivative of free surface elevation $\eta_t(x, t)$ and time derivative of surface potential $\Phi_t^s(x, t)$. Then, based on the 4th order Runge-Kutta equation, the free surface elevation $\eta(x, t + \Delta t)$ and surface potential $\Phi^S(x, t + \Delta t)$ at the next time step will be obtained and utilized to calculate the value of modal amplitudes for iteration.

For calculating the temporal evolution of the resonant wave amplitude, the periodic rippled bottoms are set over a total length of the computation domain due to the periodic boundary in the HOS model. The input data for HOS simulation in this study includes the spatial points distribution and time step and evolution time information, as well as the initial free surface profile and rippled bottoms profile, which are nondimensional.

3. Numerical Simulation of Temporal Evolution for Resonant Wave Amplitude above Infinite Patch by HOS and its Comparison with the Theory

In this section, the temporal evolution of resonant wave amplitude for all six triad resonant combinations will be numerically simulated and compared with nonlinear theoretical solutions based on multiple-scale expansion perturbation analysis, which are referred to in Appendices A and B.

For the ripples' configuration during the temporal evolution simulation in HOS, the harmonic rippled bottoms are fulfilled in the whole computational domain, which could capture the resonance-related wave evolution above the infinite extended rippled patch due to the periodic conditions on both sides of the computational domain in this numerical model.

For HOS configuration with a general triad combination $k_m - k_n = k_b$ and $\omega_m = \omega_n$, the initial free-surface disturbance wave component k_n is given in prior with amplitude a_n . There was no other free-surface wave component k_m that existed initially. Then, the amplitude temporal variation $A_m(t)$ will be extracted from the HOS simulation results.

Correspondingly, for the theoretical solution, the corresponding initial conditions for $A_m(t)$ at $t = 0$ are as below,

$$A_m(0) = 0 \tag{15}$$

$$\left. \frac{dA_m(t)}{dt} \right|_{t=0} = A_n(t)\mathbb{P} = a_n\mathbb{P} \tag{16}$$

The solution of Equation (A1) (without spatial derivative and variables) of $A_m(t)$ with its boundary conditions (15) and (16) is,

$$A_m(t) = \frac{a_n\mathbb{P}}{\gamma} \sin \gamma t \tag{17}$$

The other wave component k_n , which is given in prior with initial amplitude a_n , its initial conditions at $t = 0$ is as below.

$$A_n(0) = a_n \tag{18}$$

$$\left. \frac{dA_n(t)}{dt} \right|_{t=0} = A_m(t)\mathbb{Q} = 0 \tag{19}$$

The solution of Equation (A2) (without spatial derivative and variables) of $A_n(t)$ with its initial conditions (18) and (19) is,

$$A_n(t) = a_n \cos \gamma t \tag{20}$$

The detailed comparisons between HOS and theoretical solutions are presented below for all six triad resonant combinations. It should be noted that the total length of the computational domain in HOS is equal to the total length of rippled patch, so the bottom boundary condition is fully periodic as infinite patch during the simulation process. Moreover, due to the numerical simulation being intended to capture the triad resonant interaction as the second order, the nonlinear order M in HOS is set as two, correspondingly. The wave number and flow velocity values applied afterwards are selected from the parameter's domain of all six triad resonance combinations (as referred to in [2] Figure 3).

3.1. Triad Resonant Combination (1) $k_3 - k_1 = k_b$

For the selected condition from the triad resonant combination (1) for temporal evolution validation, the triad resonant condition is $k_3 - k_1 = k_b$, and the wave component k_3 is given in prior as the initial free surface disturbance wave component. The water depth h and flow velocity U are 0.192 m and 0.2586 m/s, respectively. The corresponding Froude number is 0.1884.

The resonant wave component k_3 has the wavelength $L_3 = 0.9975$ m and initial wave amplitude $A_3(0) = 7.9379 \times 10^{-5}$ with steepness $k_3 A_3 = 0.0005$. The other free-surface wave component, k_1 , induced by resonant interaction, has the wavelength $L_1 = 0.3160$ m. The wave period of the resonant free-surface wave component is 0.7125 s. The bottom wavelength L_b is 0.24 m and amplitude A_b is 0.005 m with the corresponding bottom steepness $k_b A_b$ of 0.1309.

For the satisfaction of the periodic boundary in HOS, the total length of the computation domain is set as $L = 31.92$ m, which is 133 integral times that of the bottom wavelength L_b , 101 integral times that of L_1 , and 32 integral times that of L_3 .

As for the configuration of the numerical model, there are 8192 (2^{13}) spatial points in this computational domain, and the distance between neighboring spatial sampling points is $\Delta x = 0.0039$ m. The time step Δt is set as 0.0104 s. The total time steps during the whole computation process is 25,600 (total calculation time as 265.01 s).

Figure 1 is the comparison of the amplitude of free-surface resonant wave components k_3 (initially given) and k_1 (generated by resonance) between HOS simulation and multiple-scale expansion perturbation analysis. The HOS results present the harmonic temporal variation pattern (temporally stable), which compares well with the multiple-scale expansion (nonlinear) solutions.

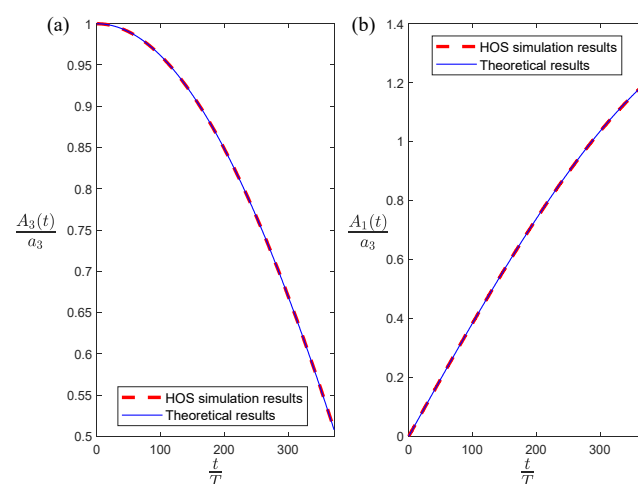


Figure 1. Resonant wave components' amplitude temporal evolution comparison for triad combination (1); (a) k_3 wave component dimensionless amplitude $A_3(t)/a_3$ temporal evolution comparison, Multiple-scale expansion solution (Blue line), HOS simulations (Red dash line); (b) k_1 wave component dimensionless amplitude $A_1(t)/a_3$ temporal evolution comparison, Multiple-scale expansion solution (Blue line), HOS simulations (Red dash line); T is the wave period, a_3 is the initial wave amplitude of k_3 wave component.

However, the traditional temporal instability analysis indicates that this triad resonant combination is temporally unstable (with exponential growth), which is inconsistent with the HOS simulation and multiple-scale expansion solutions.

3.2. Triad Resonant Combination (2) $k_3 - k_2 = k_b$

For the selected condition from triad resonant combination (2) for temporal evolution validation, the triad resonant condition is $k_3 - k_2 = k_b$, and the wave component k_3 is given in prior as the initial free surface disturbance wave component. The water depth h and flow velocity U are 0.192 m and 0.4754 m/s, respectively. The corresponding Froude number is 0.3464.

The resonant wave component k_3 has the wavelength $L_3 = 2.9826$ m and initial wave amplitude $A_3(0) = 2.3019 \times 10^{-4}$ m with steepness $k_3 A_3 = 0.0005$. The other free-surface wave component k_2 induced by resonant interaction has the wavelength $L_2 = 0.2617$ m. The wave period of the resonant free-surface wave component is 1.5980 s. The bottom wavelength L_b is 0.24 m and amplitude A_b is 0.005 m with the corresponding bottom steepness $k_b A_b$ of 0.1309.

For the satisfaction of the periodic boundary in HOS, the total length of the computation domain is set as $L = 54.96$ m, which is 229 integral times that of the bottom wavelength L_b , 210 integral times of L_2 , and 19 integral times of L_3 .

As for the configuration of the numerical model, there are 8192 (2^{13}) spatial points in this computational domain, and the distance between neighboring spatial sampling points is $\Delta x = 0.0067$ m. The time step Δt is set as 0.0095 s. The total time steps during the whole computation process is 25,600 (total calculation time as 243.59 s).

Figure 2 is the comparison of the amplitude of free-surface resonant wave components k_3 (initially given) and k_2 (generated by resonance) between HOS simulation and multiple-scale expansion perturbation analysis. Similar to the triad combination (1), the HOS results of triad combination (2) present the harmonic temporal variation pattern (temporally stable), which also compares well with the multiple-scale expansion (nonlinear) solutions.

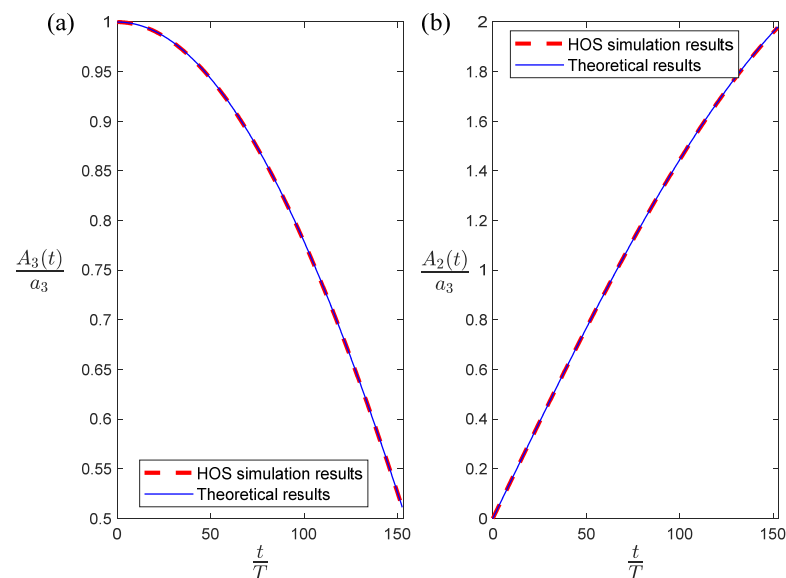


Figure 2. Resonant wave components' amplitude temporal evolution comparison for triad combination (2); (a) k_3 wave component dimensionless amplitude $A_3(t)/a_3$ temporal evolution comparison, Multiple-scale expansion solution (Blue line), HOS simulations (Red dash line); (b) k_2 wave component dimensionless amplitude $A_2(t)/a_3$ temporal evolution comparison, Multiple-scale expansion solution (Blue line), HOS simulations (Red dash line); T is the wave period, a_3 is the initial wave amplitude of k_3 wave component.

On the contrary, the traditional temporal instability analysis indicates that the triad resonant combination (2) is temporally unstable (with exponential growth), which is still inconsistent with the HOS simulation and multiple-scale expansion solutions.

3.3. Triad Resonant Combination (3) $k_4 - k_3 = k_b$

For the selected condition from triad resonant combination (3) for temporal evolution validation, the triad resonant condition is $k_4 - k_3 = k_b$, and the wave component k_3 is given in prior as the initial free surface disturbance wave component. The water depth h and flow velocity U are 0.192 m and 0.9634 m/s, respectively. The corresponding Froude number is 0.7020.

The resonant wave component k_3 has the wavelength $L_3 = 0.9714$ m and initial wave amplitude $A_3(0) = 7.7298 \times 10^{-5}$ m with steepness $k_3 A_3 = 0.0005$. The other free-surface wave component, k_4 , induced by resonant interaction has the wavelength $L_4 = 0.1924$ m. The wave period of the resonant free-surface wave component is 0.4634 s. The bottom wavelength L_b is 0.24 m and amplitude A_b is 0.005 m with the corresponding bottom steepness $k_b A_b$ of 0.1309.

For the satisfaction of the periodic boundary in HOS, the total length of the computation domain is set as $L = 143.76$ m, which is 599 integral times that of the bottom wavelength L_b , 148 integral times that of L_3 , and 747 integral times that of L_4 .

As for the configuration of the numerical model, there are 16384 (2^{14}) spatial points in this computational domain, and the distance between neighboring spatial sampling points is $\Delta x = 0.0088$ m. The time step Δt is set as 0.0193 s. The total time steps during the whole computation process is 5120 (total calculation time as 98.73 s).

Figure 3 is the comparison of the amplitude of free-surface resonant wave components k_3 (initially given) and k_4 (generated by resonance) between HOS simulation and the multiple-scale expansion perturbation analysis. Different from the triad combinations (1) and (2), the HOS results of the triad combination (3) present an exponential temporal variation pattern (temporally unstable), which also compares well with the multiple-scale expansion (nonlinear) solutions.

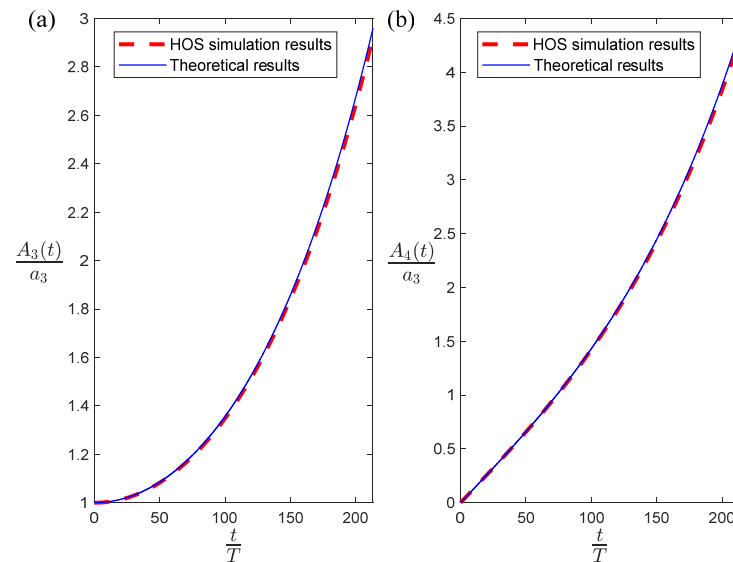


Figure 3. Resonant wave components’ amplitude temporal evolution comparison for triad combination (3); (a) k_3 wave component dimensionless amplitude $A_3(t)/a_3$ temporal evolution comparison, Multiple-scale expansion solution (Blue line), HOS simulations (Red dash line); (b) k_4 wave component dimensionless amplitude $A_4(t)/a_3$ temporal evolution comparison, Multiple-scale expansion solution (Blue line), HOS simulations (Red dash line); T is the wave period, a_3 is the initial wave amplitude of k_3 wave component.

This triad resonant combination is the situation discussed by Yih [11]. The traditional temporal instability analysis indicates that the triad resonant combination (3) is temporally unstable (also with exponential growth), which coincides with HOS simulation and multiple-scale expansion solutions.

3.4. Triad Resonant Combination (4) $k_4 - k_2 = k_b$

For the selected condition from triad resonant combination (4) for temporal evolution validation, the triad resonant condition is $k_4 - k_2 = k_b$, and the wave component k_2 is given in prior as the initial free surface disturbance wave component. The water depth h and flow velocity U are 0.192 m and 0.8311 m/s, respectively. The corresponding Froude number is 0.6056.

The resonant wave component k_2 has the wavelength $L_2 = 0.7984$ m and initial wave amplitude $A_2(0) = 6.3532 \times 10^{-5}$ m with steepness $k_2 A_2 = 0.0005$. The other free-surface wave component, k_4 , induced by resonant interaction has the wavelength $L_4 = 0.3432$ m. The wave period of the resonant free-surface wave component is 3.4380 s. The bottom wavelength L_b is 0.24 m and amplitude A_b is 0.005 m with the corresponding bottom steepness $k_b A_b$ of 0.1309.

For the satisfaction of the periodic boundary in HOS, the total length of the computation domain is set as $L = 39.12$ m, which is 163 integral times that of the bottom wavelength L_b , 49 integral times that of L_2 , and 114 integral times that of L_4 .

As for the configuration of the numerical model, there are 8192 (2^{13}) spatial points in this computational domain, and the distance between neighboring spatial sampling points is $\Delta x = 0.0048$ m. The time step Δt is set as 0.0083 s. The total time steps during the whole computation process is 25,600 (total calculation time as 212.93 s).

Figure 4 is the comparison of the amplitude of free-surface resonant wave components k_2 (initially given) and k_4 (generated by resonance) between HOS simulation and multiple-scale expansion perturbation analysis. The HOS results of triad combination (4) present the exponential temporal variation pattern (temporally unstable), which also compares well with the multiple-scale expansion (nonlinear) solutions. It should be noted that although the temporal variation pattern presents linear growth in Figure 4b, it also presents exponential growth on the longer time scale.

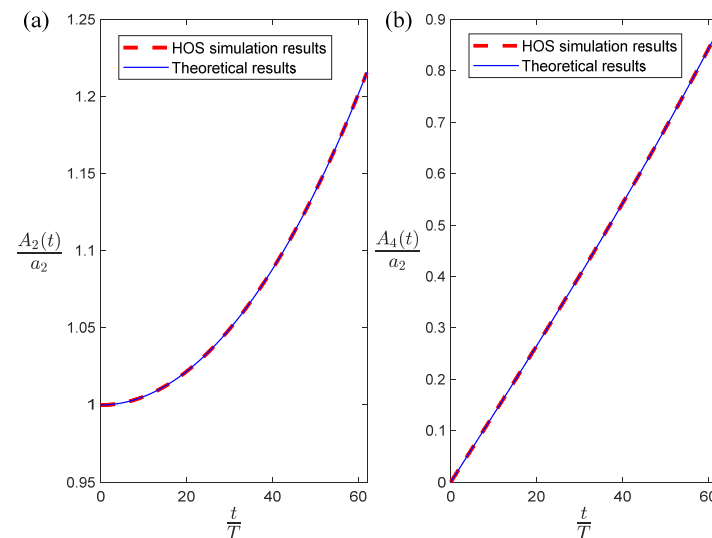


Figure 4. Resonant wave components' amplitude temporal evolution comparison for triad combination (4); (a) k_2 wave component dimensionless amplitude $A_2(t)/a_2$ temporal evolution comparison, Multiple-scale expansion solution (Blue line), HOS simulations (Red dash line); (b) k_4 wave component dimensionless amplitude $A_4(t)/a_2$ temporal evolution comparison, Multiple-scale expansion solution (Blue line), HOS simulations (Red dash line); T is the wave period, a_2 is the initial wave amplitude of k_2 wave component.

The traditional temporal instability analysis indicates that the triad resonant combination (4) is temporally unstable (also with exponential growth), which coincides with the HOS simulation and multiple-scale expansion solutions.

3.5. Triad Resonant Combination (5) $k_4 - k_1 = k_b$

For the selected condition from triad resonant combination (5) for temporal evolution validation, the triad resonant condition is $k_4 - k_1 = k_b$, and the wave component k_1 is given in prior as the initial free surface disturbance wave component. The water depth h and flow velocity U are 0.192 m and 0.7695 m/s, respectively. The corresponding Froude number is 0.5607.

The resonant wave component k_1 has the wavelength $L_1 = 1.3900$ m and initial wave amplitude $A_1(0) = 1.1061 \times 10^{-4}$ m with steepness $k_1 A_1 = 0.0005$. The other free-surface wave component, k_4 , induced by resonant interaction has the wavelength $L_4 = 0.2901$ m. The wave period of the resonant free-surface wave component is 3.0003 s. The bottom wavelength L_b is 0.24 m and amplitude A_b is 0.005 m with the corresponding bottom steepness $k_b A_b$ of 0.1309.

For the satisfaction of the periodic boundary in HOS, the total length of the computation domain is set as $L = 33.36$ m, which is 139 integral times that of the bottom wavelength L_b , 24 integral times that of L_1 , and 115 integral times that of L_4 .

As for the configuration of the numerical model, there are 4096 (2^{12}) spatial points in this computational domain, and the distance between neighboring spatial sampling points is $\Delta x = 0.0081$ m. The time step Δt is set as 0.0154 s. The total time steps during the whole computation process is 51,200 (total calculation time as 788.58 s).

Figure 5 is the comparison of the amplitude of free-surface resonant wave components k_1 (initially given) and k_4 (generated by resonance) between HOS simulation and multiple-scale expansion perturbation analysis. The HOS results of triad combination (5) present the exponential temporal variation pattern (temporally unstable), which also compares well with the multiple-scale expansion (nonlinear) solutions.

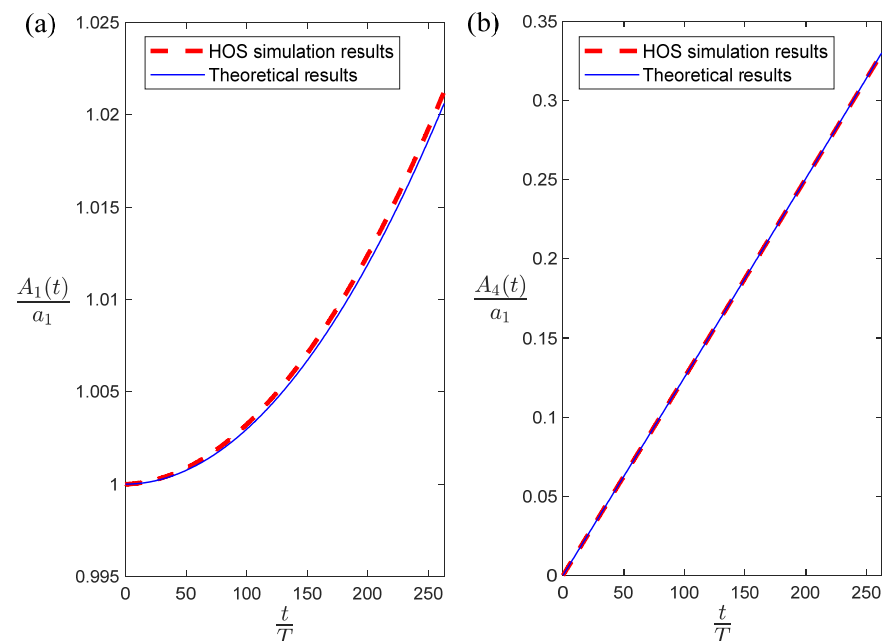


Figure 5. Resonant wave components' amplitude temporal evolution comparison for triad combination (5); (a) k_1 wave component dimensionless amplitude $A_1(t)/a_1$ temporal evolution comparison, Multiple-scale expansion solution (Blue line), HOS simulations (Red dash line); (b) k_4 wave component dimensionless amplitude $A_4(t)/a_1$ temporal evolution comparison, Multiple-scale expansion solution (Blue line), HOS simulations (Red dash line); T is the wave period, a_1 is the initial wave amplitude of k_1 wave component.

On the contrary, the traditional temporal instability analysis indicates that the triad resonant combination (5) is temporally stable (with a harmonic temporal variation pattern), which is inconsistent with HOS simulation and multiple-scale expansion solutions.

3.6. Triad Resonant Combination (6) $k_1 - k_2 = k_b$

For the selected condition from triad resonant combination (6) for temporal evolution validation, the triad resonant condition is $k_1 - k_2 = k_b$, and the wave component k_2 is given in prior as the initial free surface disturbance wave component. The water depth h and flow velocity U are 0.192 m and 0.4878 m/s, respectively. The corresponding Froude number is 0.3554.

The resonant wave component k_2 has the wavelength $L_2 = 0.2133$ m and initial wave amplitude $A_2(0) = 1.6976 \times 10^{-5}$ m with steepness $k_2 A_2 = 0.0005$. The other free-surface wave component, k_1 , induced by resonant interaction has the wavelength $L_1 = 1.9200$ m. The wave period of the resonant free-surface wave component is 2.3871 s. The bottom wavelength L_b is 0.24 m and amplitude A_b is 0.005 m with the corresponding bottom steepness $k_b A_b$ of 0.1309.

For the satisfaction of the periodic boundary in HOS, the total length of the computation domain is set as $L = 145.92$ m, which is 608 integral times that of the bottom wavelength L_b , 76 integral times that of L_1 , and 684 integral times that of L_2 .

As for the configuration of the numerical model, there are 8192 (2^{13}) spatial points in this computational domain, and the distance between neighboring spatial sampling points is $\Delta x = 0.0178$ m. The time step Δt is set as 0.0049 s. The total time steps during the whole computation process is 30,720 (total calculation time as 149.95 s).

Figure 6 is the comparison of the amplitude of free-surface resonant wave components k_2 (initially given) and k_1 (generated by resonance) between HOS simulation and multiple-scale expansion perturbation analysis. The HOS results of triad combination (6) present the harmonic temporal variation pattern (temporally stable), which also compares well with the multiple-scale expansion (nonlinear) solutions.

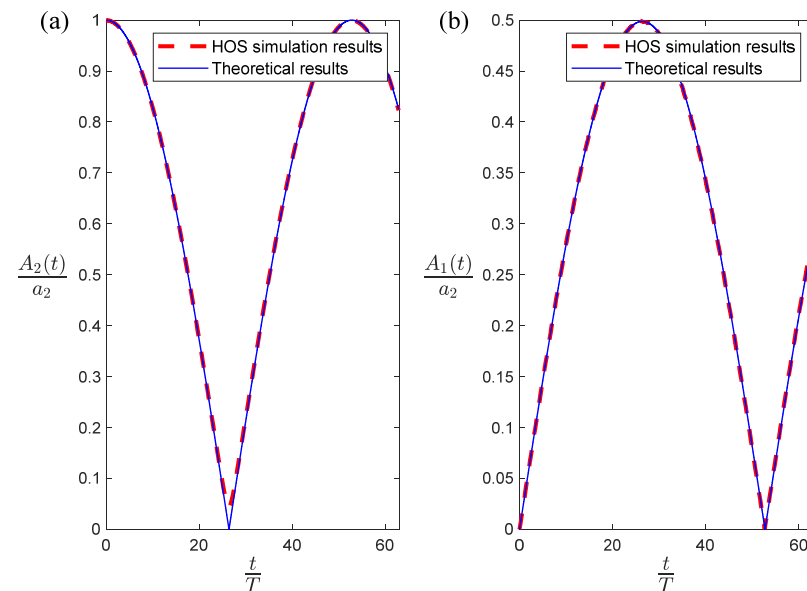


Figure 6. Resonant wave components’ amplitude temporal evolution comparison for triad combination (6); (a) k_2 wave component dimensionless amplitude $A_2(t)/a_2$ temporal evolution comparison, Multiple-scale expansion solution (Blue line), HOS simulations (Red dash line); (b) k_1 wave component dimensionless amplitude $A_1(t)/a_2$ temporal evolution comparison, Multiple-scale expansion solution (Blue line), HOS simulations (Red dash line); T is the wave period, a_2 is the initial wave amplitude of k_2 wave component.

The traditional temporal instability analysis indicates that the triad resonant combination (4) is temporally stable (with harmonic temporal variation pattern), which coincides with the HOS simulation and multiple-scale expansion solutions.

It should be noted that this triad resonant combination (6) corresponds to the generation of upstream-propagating waves in flume experiments. Although this triad combination is temporally stable, the intensive free surface waves could still be stimulated due to the combined condition of spatial exponential growth behavior and the critical flow condition of wave energy stagnation.

3.7. Overall Comparison between HOS Results and Theoretical Analysis

For better comparison, the resonant condition, phase and energy propagating directions, and temporal evolution behaviors (calculated by HOS simulation, multiple-scale expansion, and traditional temporal instability analysis) for all six triad resonant combinations have been summarized and organized in Table 1.

Table 1. Summarization and comparisons of temporal evolution behavior for six triad resonant combinations among HOS simulation results (this study), multiple-scale expansion analysis [2] (Appendix A), and traditional temporal instability analysis [14] (Appendix B).

Triad Resonant Combination	Phase Propagating Direction	Energy Propagating Direction	HOS Simulation Results	Multiple-Scale Expansion Analysis	Temporal Instability Analysis
No.1 $k_3 - k_1 = k_b$	k_3 : Downstream k_1 : Upstream	k_3 : Downstream k_1 : Upstream	Stable	Stable	Unstable
No.2 $k_3 - k_2 = k_b$	k_3 : Downstream k_2 : Upstream	k_3 : Downstream k_2 : Downstream	Stable	Stable	Unstable
No.3 $k_4 - k_3 = k_b$	k_4 : Downstream k_3 : Downstream	k_4 : Downstream k_3 : Downstream	Unstable	Unstable	Unstable
No.4 $k_4 - k_2 = k_b$	k_4 : Downstream k_2 : Upstream	k_4 : Downstream k_2 : Downstream	Unstable	Unstable	Unstable
No.5 $k_4 - k_1 = k_b$	k_4 : Downstream k_1 : Upstream	k_4 : Downstream k_1 : Upstream	Unstable	Unstable	Stable
No.6 $k_1 - k_2 = k_b$	k_1 : Upstream k_2 : Upstream	k_1 : Upstream k_2 : Downstream	Stable	Stable	Stable

It reveals that the HOS simulation results for temporal evolution behavior are always consistent with the theoretical analysis by multiple-scale expansion for all six triad combinations, which could be confirmed on the basis of such cross-validation. However, there are contradictions with the results with traditional temporal instability analysis for triad combinations (1), (2), and (5). If the study of triad resonance behaviors involves these three combinations, one should be cautious in the analysis of their temporal evolution behaviors.

4. Discussion and Conclusions

In this study, the High-Order Spectral (HOS) method is applied to simulate the temporal evolution behavior of triad resonant wave components' amplitude for steady free-surface flow over rippled bottoms. The numerical calculation results compare well with the multiple-scale expansion perturbation solutions as the cross-validation.

Both the numerical and theoretical (multiple-scale expansion) work reveals the consistent temporal evolution behaviors. In addition, this work confirms the temporal evolution behavior for all six triad resonant combinations in which triad resonant combinations (3), (4), and (5) are unstable with exponential temporal growth for both free-surface resonant wave components involved, and triad resonant combinations (1), (2), and (6) are stable with harmonic temporal growth and limited amplitude values. Moreover, it also reveals that all three unstable triad resonant combinations involve the free-surface wave component k_4 , which is not easy to be observed and needs further investigation.

It should be noted that the numerical and theoretical work in this paper is still limited to the second order, which corresponds to the triad resonant interaction. In future work, the higher order effects for the resonant interaction involved need to be studied, and the further theoretical mechanisms for the differences between tradition instability analysis and multiple-scale expansion perturbation analysis will be discussed in detail with more mathematical methods [28–31]. Moreover, the experimental observation of wave component k_4 in the ambient current and its connection with the temporal instability behavior need to be identified.

Author Contributions: Conceptualization, J.F., A.T. and J.Z.; methodology, A.T. and J.Z.; software, J.F. and J.P.; validation, A.T. and J.P.; formal analysis, J.F.; investigation, J.F.; writing—original draft preparation, J.F.; writing—review and editing, J.F.; visualization, J.F. and J.P.; supervision, A.T. and J.Z. All authors have read and agreed to the published version of the manuscript.

Funding: This research was supported by the National Natural Science Foundation of China (Grant No. 52101308), the National Natural Science Foundation of China (Grant No. 52271271), and the Fundamental Research Funds for the Central Universities (Grant No. B220202080).

Institutional Review Board Statement: Not applicable.

Informed Consent Statement: Not applicable.

Data Availability Statement: Not applicable.

Conflicts of Interest: The authors declare no conflict of interest.

Appendix A. Theoretical Solution of Triad Resonance by Multiple-Scale Expansion Analysis

The amplitudes of resonant wave components could be solved theoretically by multiple-scale expansion perturbation analysis. The decoupled equations of resonant wave amplitude $A_m(x, t)$ and $A_n(x, t)$ are obtained [2] and restated as below.

$$\frac{\partial^2 A_m(x, t)}{\partial t^2} + (C_{mg} + C_{ng}) \frac{\partial^2 A_m(x, t)}{\partial x \partial t} + C_{mg} C_{ng} \frac{\partial^2 A_m(x, t)}{\partial x^2} + \mathbb{P} \mathbb{Q} A_m(x, t) = 0 \quad (A1)$$

$$\frac{\partial^2 A_n(x, t)}{\partial t^2} + (C_{mg} + C_{ng}) \frac{\partial^2 A_n(x, t)}{\partial x \partial t} + C_{mg} C_{ng} \frac{\partial^2 A_n(x, t)}{\partial x^2} + \mathbb{P} \mathbb{Q} A_n(x, t) = 0 \quad (A2)$$

in which C_{mg} and C_{ng} are the group velocities of resonant wave components. The parameters \mathbb{P} and \mathbb{Q} are,

$$\mathbb{P} = \left[\frac{gbk_m k_n}{4(\omega - k_n U) \cosh k_m h \cosh k_n h} + \frac{Ubk_b}{2g(g \sinh k_b h - U^2 k_b \cosh k_b h)} \mathbb{M} \right] \quad (A3)$$

$$\mathbb{Q} = \left[\frac{gbk_m k_n}{4(\omega - k_m U) \cosh k_m h \cosh k_n h} + \frac{Ubk_b}{2g(g \sinh k_b h - U^2 k_b \cosh k_b h)} \mathbb{N} \right] \quad (A4)$$

Thus, the parameters \mathbb{M} and \mathbb{N} in the expressions of \mathbb{P} and \mathbb{Q} are given as follows,

$$\mathbb{M} = \left\{ \begin{aligned} &gk_n \frac{\omega - (k_n + k_b)U}{\omega - k_n U} (U^2 k_b \tanh k_n h - g) \\ &+ \frac{1}{2} \left[\frac{Ug^2 k_n^2}{\omega - k_n U} \frac{1}{\cosh^2 k_n h} + k_b (U^4 k_b^2 - g^2) \right] \end{aligned} \right\} \quad (A5)$$

$$\mathbb{N} = \left\{ \begin{aligned} &-gk_m \frac{\omega - (k_m - k_b)U}{\omega - k_m U} (U^2 k_b \tanh k_m h + g) \\ &+ \frac{1}{2} \left[\frac{Ug^2 k_m^2}{\omega - k_m U} \frac{1}{\cosh^2 k_m h} - k_b (U^4 k_b^2 - g^2) \right] \end{aligned} \right\} \quad (A6)$$

For the temporal evolution solutions of resonant wave amplitude, the equations could be obtained by ignoring the spatial derivative and variables, and could be solved by initial

conditions. The temporal instability behavior could be revealed by parameter \mathbb{PQ} [2], in which the resonant wave is temporally unstable if $\mathbb{PQ} < 0$ and is stable if $\mathbb{PQ} \geq 0$.

Appendix B. Traditional Temporal Instability Analysis of Triad Resonant Modes

In previous research on steady flow over rippled bottoms, the temporal variation characteristics of free-surface wave components were investigated utilizing instability analysis [14]. Based on the dimensionless boundary value problem (BVP), the steady and unsteady disturbance terms of the velocity potential and free surface elevation are defined separately. After obtaining the BVP for the disturbance terms of velocity potential, the dimensionless frequency σ ($\sigma = \omega h/U$) is expanded in a power series as $\sigma = \lambda_0 + a\lambda_1 + a^2\lambda_2^2 + \dots$. Although the leading order term λ_0 in this series corresponds to the frequency of disturbance wave without triad resonant interaction, whether the next-order term λ_1 is real or imaginary will determine the instability. The expression of λ_1^2 given are presented as below [14].

$$\lambda_1^2 = \frac{mm'b^2\mathbb{G}\mathbb{H}}{16(\lambda_0 - m)(\lambda_0 - m')} \tag{A7}$$

in which m is the dimensionless wavenumber as $m = kh$, and is the amplitude of stationary waves given as below,

$$b = \frac{am_b}{m_b \cosh m_b - F^{-2}\sinh m_b} \tag{A8}$$

in which, m_b and a are dimensionless wavenumber and amplitude of rippled bottoms separately, and F is the Froude number.

The parameters \mathbb{G} and \mathbb{H} are as follows,

$$\mathbb{G} = (\lambda_0 - m)^2 \tanh m' + F^{-2}(2\lambda_0 - 2m - m') \tag{A9}$$

$$\mathbb{H} = (\lambda_0 - m)^2 \tanh m' + F^{-2}(2\lambda_0 - 2m - m') \tag{A10}$$

Based on expression for λ_1^2 , if the value of λ_1^2 is negative (or positive), the wave components involved in triad resonance for flow over rippled bottoms are unstable (or stable). Moreover, the situation for the value of λ_0 defined as negative under different definitions [14] has also been taken into consideration and calculated.

References

- Raj, R.; Guha, A. On Bragg Resonances and Wave Triad Interactions in Two-Layered Shear Flows. *J. Fluid Mech.* **2019**, *867*, 482–515. [CrossRef]
- Fan, J.; Zheng, J.; Tao, A.; Liu, Y. Upstream-Propagating Waves Induced by Steady Current over a Rippled Bottom: Theory and Experimental Observation. *J. Fluid Mech.* **2021**, *910*, A49. [CrossRef]
- Choi, W.; Chabane, M.; Taklo, T.M.A. Two-Dimensional Resonant Triad Interactions in a Two-Layer System. *J. Fluid Mech.* **2021**, *907*, A5. [CrossRef]
- Lamb, H. *Hydrodynamics*; Cambridge University Press: Cambridge, UK, 1932.
- Kennedy, J.F. The Mechanics of Dunes and Antidunes in Erodible-Bed Channels. *J. Fluid Mech.* **1963**, *16*, 521–544. [CrossRef]
- Mei, C.C. Steady Free Surface Flow over Wavy Bed. *J. Eng. Mech.* **1969**, *95*, 1393–1402. [CrossRef]
- Mizumura, K. Free-Surface Profile of Open-Channel Flow with Wavy Boundary. *J. Hydraul. Eng.* **1995**, *121*, 533–539. [CrossRef]
- Phillips, O.M. *The Dynamics of the Upper Ocean*; Cambridge University Press: Cambridge, UK, 1966.
- Hasselmann, K. A Criterion for Nonlinear Wave Stability. *J. Fluid Mech.* **1967**, *30*, 737–739. [CrossRef]
- Whitham, G.B. Non-linear dispersion of water waves. *J. Fluid Mech.* **1967**, *27*, 399–412. [CrossRef]
- Yih, C.S. Instability of Surface and Internal Waves. In *Advances in Applied Mechanics*; Yih, C.-S., Ed.; Elsevier: Amsterdam, The Netherlands, 1976; Volume 16, pp. 369–419.
- Mchugh, J.P. The Stability of Stationary Waves in a Wavy-Walled Channel. *J. Fluid Mech.* **1988**, *189*, 491–508. [CrossRef]
- Mei, C.C.; Stiassnie, M.; Yue, D.K.P. *Theory and Applications of Ocean Surface Waves*; World Scientific: Singapore, 2005.
- McHugh, J.P. The Stability of Capillary-Gravity Waves on Flow over a Wavy Bottom. *Wave Motion* **1992**, *16*, 23–31. [CrossRef]
- Kyotoh, H.; Fukushima, M. Upstream-Advancing Waves Generated by a Current over a Sinusoidal Bed. *Fluid Dyn. Res.* **1997**, *21*, 1–28. [CrossRef]

16. Fan, J.; Zheng, J.; Tao, A.; Yu, H.; Wang, Y. Experimental Study on Upstream-Advancing Waves Induced by Currents. *J. Coast. Res.* **2016**, *75*, 846–850. [[CrossRef](#)]
17. Zakharov, V.E. Stability of periodic waves of finite amplitude on the surface of a deep fluid. *J. Appl. Mech. Tech. Phys.* **1968**, *9*, 190–194. [[CrossRef](#)]
18. Phillips, O.M. On the dynamics of unsteady gravity waves of finite amplitude Part 1. The elementary interactions. *J. Fluid Mech.* **1960**, *9*, 193–217. [[CrossRef](#)]
19. Dommermuth, D.G.; Yue, D.K.P. A High-Order Spectral Method for the Study of Nonlinear Gravity Waves. *J. Fluid Mech.* **1987**, *184*, 267–288. [[CrossRef](#)]
20. West, B.J.; Brueckner, K.A.; Janda, R.S.; Milder, D.M.; Milton, R.L. A new numerical method for surface hydrodynamics. *J. Geophys. Res.* **1987**, *92*, 11803–11824. [[CrossRef](#)]
21. Liu, Y.; Dommermuth, D.G.; Yue, D.K.P. A High-Order Spectral Method for Nonlinear Wave–Body Interactions. *J. Fluid Mech.* **1992**, *245*, 115. [[CrossRef](#)]
22. Liu, Y. *Nonlinear Wave Interactions with Submerged Obstacles with or without Current*; Massachusetts Institute of Technology: Singapore, 1994.
23. Liu, Y.; Yue, D.K.P. On Generalized Bragg Scattering of Surface Waves by Bottom Ripples. *J. Fluid Mech.* **1998**, *356*, 297–326. [[CrossRef](#)]
24. Peng, J.; Tao, A.; Fan, J.; Zheng, J.; Liu, Y. On the Downshift of Wave Frequency for Bragg Resonance. *China Ocean Eng.* **2022**, *36*, 76–85. [[CrossRef](#)]
25. Zhang, H.; Tao, A.; Tu, J.; Su, J.; Xie, S. The Focusing Waves Induced by Bragg Resonance with V-Shaped Undulating Bottom. *J. Mar. Sci. Eng.* **2021**, *9*, 708. [[CrossRef](#)]
26. Tao, A.; Xie, S.; Wu, D.; Fan, J.; Yang, Y. The Effects on Water Particle Velocity of Wave Peaks Induced by Nonlinearity under Different Time Scales. *J. Mar. Sci. Eng.* **2021**, *9*, 748. [[CrossRef](#)]
27. Qin, S.; Fan, J.; Zhang, H.; Su, J.; Wang, Y. Flume Experiments on Energy Conversion Behavior for Oscillating Buoy Devices Interacting with Different Wave Types. *J. Mar. Sci. Eng.* **2021**, *9*, 852. [[CrossRef](#)]
28. Liang, B.; Ge, H.; Zhang, L.; Liu, Y. Wave resonant scattering mechanism of sinusoidal seabed elucidated by Mathieu instability theorem. *Ocean Eng.* **2020**, *218*, 108238. [[CrossRef](#)]
29. Rasham, T.; De La Sen, M. A novel study for hybrid pair of multivalued dominated mappings in b-multiplicative metric space with applications. *J. Inequal Appl.* **2022**, *107*, 1–15. [[CrossRef](#)]
30. Rasham, T.; Nazam, M.; Aydi, H.; Shoaib, A.; Park, C.; Lee, J.R. Hybrid pair of multivalued mappings in modular-like metric spaces and applications. *AIMS Math.* **2022**, *7*, 10582–10595. [[CrossRef](#)]
31. Gamal, M.; Rasham, T.; Cholamjiak, W.; Shi, F.G.; Park, C. New iterative scheme for fixed point results of weakly compatible maps in multiplicative GM–metric space via various contractions with application. *AIMS Math.* **2022**, *7*, 13681–13703. [[CrossRef](#)]